

Collapse assessment and seismic performance factors in tall tube-in-tube diagrid buildings

Alireza Khatami^a, Mahdi Heshmati^b and Ali Akbar Aghakouchak*

Department of Civil and Environmental Engineering, Tarbiat Modares University, Tehran, Iran

(Received May 5, 2020, Revised August 26, 2020, Accepted September 14, 2020)

Abstract. Diagrid structures have been introduced as a fairly modern lateral load-resisting system in the design of high-rise buildings. In this paper, a novel diagrid system called tube-in-tube diagrid building is introduced and assessed through pushover and incremental dynamic analyses. The main objectives of this paper are to find the optimum angle of interior and exterior diagrid tube and evaluate the efficiency of diagrid core on the probability of collapse comparing to the conventional diagrid system. Finally, the seismic performance factors of the proposed system are validated according to the FEMA P695 methodology. To achieve these, 36-story diagrid buildings with various external and internal diagonal angles are designed and then 3-D nonlinear models of these structures developed in PERFORM-3D. The results show that weight of steel material highly depends on diagonal angle of exterior tube. Adding diagrid core generally increases the over-strength factor and collapse margin ratio of tall diagrid buildings confirming high seismic safety margin for tube-in-tube diagrid buildings under severe excitations. Collapse probabilities of both structural systems under MCE records are less than 10%. Finally, response modification factor of 3.0 and over-strength factor of 2.0 and 2.5 are proposed for design of typical diagrid and tube-in-tube diagrid buildings, respectively.

Keywords: diagrid system; pushover; Incremental Dynamic Analysis (IDA); collapse margin ratio; FEMA P695; high-rise building

1. Introduction

Diagrid structural system is an innovative version of tubular systems, which is desirable for architectural and structural designers of tall buildings for its lattice-like aesthetics and structural effectiveness. The word “diagrid” is an abbreviation of the words “diagonal” and “grid” (Boake 2014). This system is composed of large diagonal members and horizontal ring beams creating triangular configuration, where all the conventional vertical columns are omitted. Repetitive triangular modules are distributed along the height of the diagrid building. This triangular shape of diagrid module is more stable than quadrangular form of conventional orthogonal frame and may provide greater lateral stiffness. Gravity loads and lateral forces are resisted simultaneously by the triangular shape of the diagrid system. In diagrid systems, lateral loads produce large compressive and tensile axial forces along the diagonal members. However, lateral forces in moment resisting frame (MRF) produce large bending moment and axial force in columns.

The diagrid system was first used in the 13-story IBM

building in Pittsburgh in the early 1960s (Moon *et al.* 2007). The other famous engineering applications of diagrid systems are the Swiss Re building in London, the Hearst tower in New York and the Guangzhou International Finance Center. In the past decades, extensive researches have been carried out on the nonlinear responses of tall buildings (Pejovic *et al.* 2017, Pejovic *et al.* 2018, Kamaludin *et al.* 2020), among which design optimization of diagrid systems has grown in its popularity. Moon *et al.* (2007) and Montuori *et al.* (2014) proposed an approximate methodology for preliminary design of cross-sectional area of diagonal members based on stiffness-based method and strength design criteria, respectively. Moon *et al.* (2007) concluded that for diagrid buildings with aspect ratio of 5, the optimal angle of diagonals were in the range of 55° to 65° and also increased with the rise of aspect ratio. Zhang *et al.* (20

12) studied diagrid structures in which straight diagonal angles changed from bottom to top of the building to minimize steel material consumption. They proposed optimal geometries for diagrid buildings with different aspect ratios between 3.6 to 9.0 under wind load. Also top and bottom optimum angles of diagrids having curved diagonals were studied by Zhao and Zhang (2015). Kim and Lee (2012) investigated seismic behavior of 36-story diagrid buildings using pushover and nonlinear time history analyses. They concluded that uniform diagonal angle in the range of 60° to 70° was the most efficient geometry for 36-story diagrid structure. Milana *et al.* (2015) compared seismic performance of 40-story diagrid buildings with diagonal angles of 42°, 60° and 75° and a conventional

*Corresponding author, Professor

E-mail: a_gha@modares.ac.ir

^aM.Sc. Student

E-mail: khatami.alireza.70@gmail.com

^bM.Sc. Student

E-mail: heshmati_mahdi@yahoo.com

outrigger structure using nonlinear static analysis. They indicated the weight reduction of 33% for diagrid 75° compared to that of the outrigger structure. These configurations of diagrids not only reduced the weight of structure, but also enhanced the performance of structures in terms of strength, stiffness and ductility. The diagrid 60° exhibited the best overall performance.

Montuori *et al.* (2014) evaluated the necessity of secondary bracing system (SBS) in a 90-story diagrid building to prevent excessive inter-story drift and compressive buckling of diagonals. In recent years, some researchers improved the seismic ductility, seismic performance and damping capacity of diagrid buildings under severe earthquakes. In this regard, Kim and Lee (2012) utilized buckling-restrained braces instead of conventional diagonals. Also Moghaddasi and Zhang (2013), and Li *et al.* (2019) used replaceable shear-link fuse elements to dissipate earthquake energy. Regarding the shear lag phenomenon, Leonard (2007) studied shear lag effects of 60-story diagrids with different configurations. The diagrid building experienced significantly less shear lag compared with conventional framed-tube building and the optimal angle for the diagrid system was found to be between 63.4° and 71.6°. Kim and Lee (2012) suggested that diagrid structure with circular plan produced smaller shear lag compared with square plan. Shi and Zhang (2019) proposed a simplified calculation to solve the optimal angle of diagonals and shear lag effect in preliminary design of diagrid structures. Asadi and Adeli (2018) drew a parallel between linear and nonlinear behavior of 8-, 15- and 30-story diagrid structures and conventional moment resisting frames (MRFs) and concentrically braced frames (CBFs). They concluded that diagrid were practical and efficient structural system in mid- to high-rise buildings with larger initial stiffness compared to CBFs and MRFs. Ductility of diagrids were smaller than MRFs which could be an issue for diagrids in high seismic regions.

Recent studies and achievements of diagrid systems were discussed in review papers by Asadi and Adeli (2017), and Liu *et al.* (2018). Recently, seismic performance of tall diagrid buildings have attracted the attention of researchers (Kim and Lee 2012, Milana *et al.* 2015, Asadi and Adeli 2018, Heshmati and Aghakouchak 2018, Li *et al.* 2019) in which interior core frames have been assumed to carry only gravity loads (Moon 2008, Kim and Lee 2012, Heshmati and Aghakouchak 2018, Heshmati *et al.* 2020). As a consequence of postmodern movement, the interior structural system received attentions as part of the lateral-load-resisting system in high-rise buildings (Ali and Moon 2011). But it was not a novel concept as it had been used in some buildings in the modern era (Al-Kodmany and Ali 2016). Nowadays, architects are thinking about buildings that are quite different from those of the past. Construction development and computer analyses enable us to draw complex shape buildings with inclination. Super tall diagrid buildings can be strengthened and stiffened by adding core, providing a new system similar to a tube-in-tube structures. In this regard, Moon *et al.* (2007) added braced core in diagrid buildings to improve lateral stiffness of structures. Diagrid core system offers not only great architectural



(a) The Capital Gate in UAE



(b) The Guangzhou IFC in China (Boake 2014)

Fig. 1 Application of interior diagrid tube in tall buildings

flexibility in exterior facades, but also enhances the aesthetic appeal inside of towers with elimination of bearing walls. Notable illustrations of the considered system are Capital Gate in UAE (2011) and Guangzhou IFC (2010) in China (Fig. 1) that central atriums were supported by an additional diagrid structures to provide the interior support for the floor system, in which inner and outer diagrid tubes were connected by floor beams pin-connected at their ends (Boake 2014, Boake 2016). Hence, in this study, in order to assess the benefits of diagrid core system from structural standpoint, interior gravity load bearing system is formed as diagrid core and then tube-in-tube diagrid structure is generated. Considering the fact that the variations in diagonal angles influence the results, a combination of four different angles in the outer and inner diagrid tube are taken into account. In addition, four traditional types of diagrid models without core diagrid are considered to evaluate the effects of core. As a result, 20 structural models with identical aspect ratio (height to width ratio=4.0) are established in this study. It is worth mentioning that the main variable of this study is the inclination of diagonal members in both interior and exterior frames and investigation on the effect of aspect ratio is beyond the scope of this study. Herein, in the first step the optimum angle of diagrid in internal and external tube will be determined based on the least consumed steel material with respect to the response spectrum analysis results. Following this, nonlinear static (Pushover) and incremental dynamic analyses (IDA) are used to evaluate collapse capacity of diagrid archetypes in compliance with FEMA P695

methodology under severe ground motions equivalent to maximum considered earthquake (MCE). In addition, this document has proposed a rational methodology to determine seismic performance factors for new structural systems. Finally, influences of diagrid core with different diagonal angles are discussed on the collapse probability of tube-in-tube diagrid buildings and compared with conventional diagrid buildings.

2. Brief overview of the FEMA P695 procedure

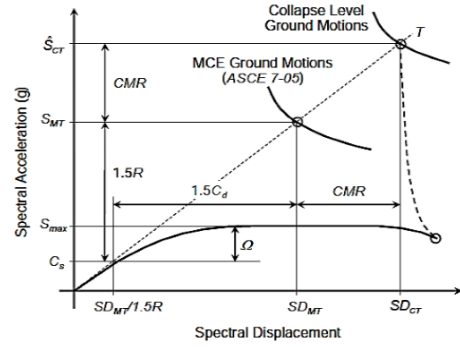
In common seismic design codes such as UBC (1997), IBC (2015) and ASCE/SEI (2016) the equivalent static lateral force analysis is employed to design structures. In this method, the magnitude of lateral forces is reduced by a reduction factor or response modification factor, R , taking advantage of the over-strength and ductility of the lateral load resisting system (Newmark and Hall 1982). The response modification factor was first introduced in ATC-3-06 (1978). Then, it was reported in ATC-19 (1995) and ATC-34 (1995) followed by a number of studies such as Miranda and Bertero 1994, Vidic *et al.* 1994, Whittaker *et al.* 1999, Freeman 1990. The response modification factor, R , is considered as a product of over-strength factor, R_μ , and ductility factor, R_0 . The over-strength factor and ductility factor are determined as follows:

$$R = R_\mu R_0 \quad R_\mu = \frac{V_e}{V_y} \quad R_0 = \frac{V_y}{V_d} \quad C_d = \frac{\Delta_{max}}{\Delta_s} \quad (1)$$

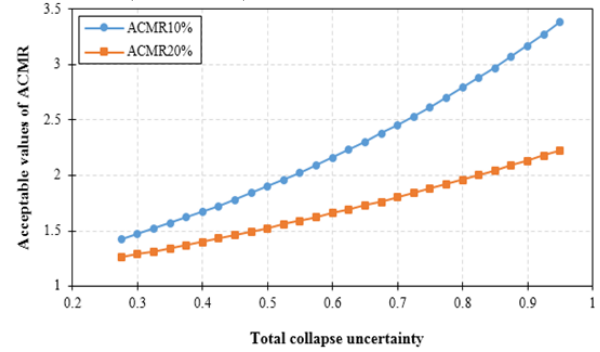
Where, V_e is maximum elastic base shear, V_y is maximum base shear of the fully-yielded system, V_d is the design base shear, Δ_{max} is the maximum lateral displacement, Δ_s is the lateral displacement corresponding to the formation of first yielding in the structural members, and C_d is the deflection amplification factor.

The FEMA P695 methodology is consistent with the primary life safety performance objective of the seismic regulations in building codes. This objective is attained by determining an acceptable low probability of collapse under Maximum Considered Earthquake (MCE) ground motions. The trial process for determining seismic performance factors by FEMA P695 comprises three major steps. These steps include characterizing system behavior and defining appropriate index archetypes, constructing nonlinear models of archetypes and conducting nonlinear static and dynamic analyses, and finally evaluating trial value of Seismic Performance Factors (SPFs) based on results of previous step considering uncertainties in each step. This methodology recommends archetypes to be assembled into performance groups that reflect variations in configuration, design gravity and seismic load intensities, structural period, and other factors that may significantly affect seismic behavior within the archetype design space.

Important design factors used in the methodology is illustrated in Fig. 2(a). This figure is consistent with pushover curve using spectral coordinates. Conversion to spectral coordinates is based on the assumption that 100% of the effective seismic weight of the structure, W , participates in fundamental mode of the system with a period of T . The ratio of the MCE spectral acceleration,



(a) Illustration of seismic performance factors as defined by FEMA P695 (June 2009)



(b) Acceptable values of ACMR (FEMA P695, 2009, Table 7-3) (June 2009)

Fig. 2 FEMA P695 parameters

S_{MT} , to the seismic response coefficient, C_s , is defined as 1.5 times the R value. The over-strength factor, Ω , for each index archetype is the ratio of the maximum strength of the fully-yielded system, S_{max} , to the seismic response coefficient, C_s (FEMA P695 June 2009).

According to this figure, the primary purpose of incremental dynamic analyses is to evaluate median collapse capacity (\hat{S}_{CT}) of structure for a given R value. The ratio of the median 5%-damped spectral acceleration of the collapse level ground motions, \hat{S}_{CT} , to the 5%-damped spectral acceleration of the MCE ground motions, S_{MT} , at the fundamental period of the structure is defined as collapse margin ratio, CMR , that can be seen in Fig. 2(b). In order to consider the shape of the spectrum of rare ground motions, the collapse margin ratio is multiplied by a factor called Spectral Shape Factor (SSF) to obtain adjusted collapse margin ratio, $ACMR$, for each archetype.

FEMA P695 defines two levels of collapse prevention objectives. the probability of collapse for MCE ground motions should be 10%, or less, on average across a performance group ($ACMR_{10\%}$) and the probability of collapse for these ground motions should be 20%, or less, for each archetype within a performance group ($ACMR_{20\%}$), based on the total system collapse uncertainty. Acceptable values of $ACMR$ ($ACMR_{10\%}$ and $ACMR_{20\%}$) versus total collapse uncertainty is plotted in Fig. 3. For a 10% collapse probability, reducing the total uncertainty from 60% to 40%, the acceptable $ACMR$ decreases from 2.16 to 1.67. If the calculated $ACMR$ is greater than the above performance objective limits, the trial value of R factor meets the collapse performance objectives. If the evaluation of

ACMR finds R factor to be unacceptable, the system needs to be re-defined by adjusting the structural design requirements, re-characterizing behavior, or re-designing with lower trial values of seismic performance factors.

In this regard, Heshmati and Aghakouchak (2018) determined seismic performance factors of 4- to 24-story diagrid buildings according to FEMA P695 methodology. Asadi and Adeli (2018) quantified SPFs of 4- to 30-story steel diagrids using nonlinear static analysis, and also evaluated performance of 4-story and 8-story diagrids using nonlinear time history analyses. Also in recent years, some scholars (Farahi and Mofid 2013, Gade and Sahoo 2016, Nobahar *et al.* 2016, Kheyroddin and Mashhadiali 2018, Özkılıç *et al.* 2018) employed this methodology to quantify SPFs of conventional structural systems.

3. Design and development of archetypes

In this study, diagrid structures are square and symmetric in plan and include 6 bays of 6.0 m in each direction. These buildings are 36-story and have a uniform story height of 4.0 m. The plan layout and elevation of the structures are shown in Fig. 3. In tube-in-tube diagrid structures all gravity loads and lateral forces are resisted by inclined members while in typical diagrid buildings the interior frame acts as a gravity frame for carrying gravity loads. Inner and outer diagrid tubes were connected by floor beams pin-connected at their ends. As shown in this figure, the diagonal slopes of 53°, 69°, 76° and 79° respectively divided the archetypes into 2-, 4-, 6- and 8- story modules that extended over the height. As it can be seen from Table 1, the archetypes were classified into 5 Performance Groups (PGs) by considering type of interior resisting frame, diagonal angle of exterior and interior resisting frames. Four diagrid structures with different diagonal slopes of 53°, 69°, 76°, 79° with horizontal line were considered, in which internal frames were assumed to be pin-connected and only carry gravity loads. Employing different combinations of aforementioned diagonal angles for exterior and interior diagrid frames provided 16 different tube-in-tube diagrid systems. The tube-in-tube diagrid structures were labeled with diagonal angles of exterior and interior tube. For instance, E69°I76° represents the model with exterior and interior diagonal angles of 69° and 76°, respectively. Also typical diagrids were named with the slope of exterior diagonals. For example, E76° shows the model with an exterior diagonal slope of 76°.

The design dead load was assumed to be 5.0 kN/m² and the values of live and partition loads were considered as 3.0 kN/m² and 1.0 kN/m² for the stories, respectively. Structural models were designed for the highest seismic design category (S_{DC}) in accordance with section 5.2.2 of FEMA P695 (June 2009). So the seismic demands were calculated with S_{DS} (short-period spectral acceleration) of 1.0g and S_{D1} (1-second spectral acceleration) of 0.6g. Approximate fundamental periods of structures were obtained by $T = C_u C_t h_n^x$, where $C_u=1.4$, $C_t=0.488$ and $x=0.75$ determined from Table 12.8-1 and 12.8-2 of ASCE 7-16. Also h_n is the structural height (in meters). In all

structures, columns and diagonal members were made of steel grade 50 with $F_y=345$ MPa and $F_u=450$ MPa. Also beams were made of steel grade 36 with $F_y=250$ MPa and $F_u=400$ MPa. All floors were assumed to be rigid. Response spectrum analysis (RSA) has been used to account for seismic loads of structures in accordance with ASCE/SEI 7-16 (2016).

As the diagrid and tubular structures are not defined as one of the seismic load resisting systems in building codes, such as ASCE 7, the values of response modification factor (R), over-strength factor (Ω_0), and deflection amplification factor (C_d) supposed to be equal to 3.0 based on previous studies (Kim, Park *et al.* 2009; Kim and Lee 2012; Kwon and Kim 2014) for initial design stage. The core and perimeter diagrids were configured to withstand both gravity and lateral forces simultaneously. Hence, inclined members, floor and ring beams were designed by following the Load and Resistance Factor Design (LRFD) provisions of AISC 360-16 (Ali and Moon 2011). This methodology was also followed by a number of researchers such as Kim and Lee (2012), Asadi *et al.* (2018), Asadi and Adeli (2018), Heshmati and Aghakouchak (2018), and Kim and Kong (2012) to design diagrid structural members. Design of archetypes for stability was adopted based on the Direct Analysis Method introduced in AISC360 (ANSI 2016). Following requirements are considered on the general stability of the archetypes: 1) Deformation of members, 2) second order effects, 3) geometric imperfections, and 4) uncertainty in stiffness and strength. Measures were taken to address the earlier requirements include: a) using notional loads to represent initial system imperfections b) utilizing a second-order analysis considering large and small deformations based on LRFD load combinations c) using reduction stiffness factor to determine the required strength d) the effective length to calculate the buckling strength of all compressive members were taken as the unbraced length (effective length factor equal to unity).

AISC 341 (2010) provides specific detailing to prevent local and global buckling of braces. These requirements are limiting width-to-thickness (D/t) and slenderness ratio (λ) of braces as well as connection detailing. In this research compactness and slenderness ratio of diagonals were met by Eq. (2) for highly ductile members.

$$D/t < 0.038 E/F_y, \quad \lambda = KL/r < 4\sqrt{E/F_y} \quad (2)$$

Where D and t are diameter and thickness of diagonals, respectively. E and F_y are modulus of elasticity and yield stress of steel, respectively. K, L and r are the effective length factor, the unbraced length and the radius of gyration of inclined members. In this research nodal connections were assumed to be fixed and have sufficient capacity to prevent failure before diagonal rupture (i.e. the principal of stronger connection, weaker component) (Asadi, Li *et al.* 2018; Heshmati and Aghakouchak 2018; 2018). Table 2 presents the results of designed sections and Demand to Capacity Ratio (DCR) for diagrid buildings in PG-1 (E53° to E79° archetypes) and PG-2 (E53°I53° to E79°I53° archetypes) to exemplify the design of archetypes. The demand to capacity ratio were obtained based on the critical

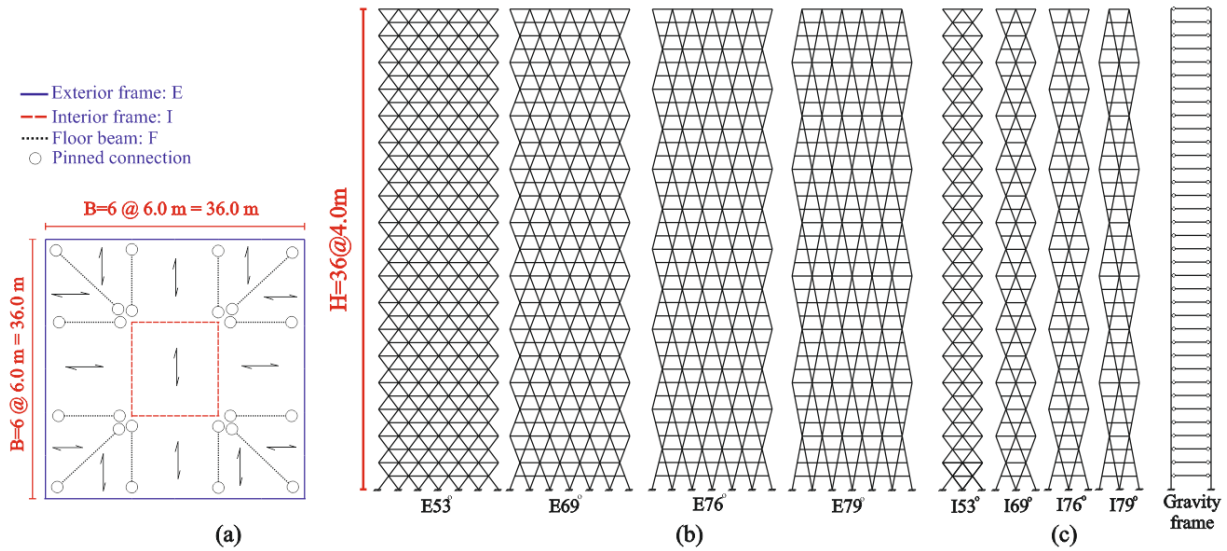


Fig. 3 Plan and elevation view of modeling structures: (a) plan and configuration of structures, (b) elevation view of exterior frames, and (c) elevation view of interior frames

Table 1: Configuration of archetypes

Group No.	Interior frame configuration	Exterior frame configuration			
		53°	69°	76°	79°
PG-1	Gravity frame	E53°	E69°	E76°	E79°
PG-2	53°	E53°I53°	E69°I53°	E76°I53°	E79°I53°
PG-3	69°	E53°I69°	E69°I69°	E76°I69°	E79°I69°
PG-4	76°	E53°I76°	E69°I76°	E76°I76°	E79°I76°
PG-5	79°	E53°I79°	E69°I79°	E76°I79°	E79°I79°

seismic load combinations suggested by FEMA P695 (Eq. (3) and Eq. (4)). Pipe and built-up box sections have been used for diagonals and columns, respectively. Also standard I-shaped sections of IPE400 and IPE 500 were used for exterior and interior ring beams of tubes, respectively. In addition, built-up plate girders (70 cm×3.0 cm×35 cm×3.0 cm) have been utilized floor beams. The same diagonal cross section was used for each module and DCR of members under design loads are near to allowable demand to capacity ratio (1.0). Variation of stories' stiffness were also checked according to ASCE 7-16 (2016) to inhibit occurrence of soft stories.

$$1.2D + E_v + E_{mh} + L \quad (3)$$

$$0.9D - E_v + E_{mh} \quad (4)$$

Where D is dead load, L is the live load, E_v is vertical seismic load, and E_{mh} is horizontal seismic load considering over-strength factor.

Finally, maximum inter-story drift ratio of structural models were restricted to allowable story drift ratio of 0.02 in accordance with ASCE 7-16 (2016). Inter-story drift variations along the height of buildings is shown in Fig. 4 and are well within the allowable range of 0.02. It can be inferred that as the angle of exterior diagonals increases, the inter-story drifts do so and also produce jumps in the curves. A good indication is provided in typical diagrid structures where the maximum inter-story drift of E53° is around 0.01, and this value rises to 0.015 when the angle of

exterior frames reaches 79°. Furthermore, as interior diagrid core provides additional stiffness, inter-story drift values of tube-in-tube diagrids are lower than typical diagrid structures. Average of maximum inter-story drift ratio for typical diagrid structures (E53° to E79°) is equal to 0.0124, however this value descends to about 0.011 for tube-in-tube diagrid structures with interior diagonal angles of 53° (E53°I53° to E79°I53°). The curves are also evident that the lower inclination in diagrid core, results in lesser peak inter-story drifts in structures. As an instance, the maximum inter-story drift of E79°I53° is around 0.011, while in case of E79°I79° the peak inter-story drift rises to 0.017. By adding diagrid core, cross section sizes of last module (story 32 to story 36) of the exterior frame for E79°I79° were obtained smaller than those for E79°. Since the exterior frame provides main contribution to lateral stiffness, the inter-story drift ratios of last module for E79°I79° obtained greater than E79° due to the smaller section sizes for diagonals. In addition, although in the remaining cases the peak inter-story drifts are the same, the distribution of inter-story drift values in the lower modules of PG-5 archetypes are smaller than PG-1 archetypes.

Eigenvalue analysis were conducted and dynamic characteristics of the diagrid structures are presented in Table 3. The natural period of structures increase with increasing the diagonal slope. Also according to Chinese code (2001) recommendation, in order to avoid excessive structural torsion, the ratio of first torsional mode and the first translational mode should be less than 0.85 which is well-established in these archetypes.

Table 2 Section sizes and DCRs for PG-1 and PG-2 (All dimensions are in cm)

Module	Diagrid frame - Pipe sections (D×t)				Interior gravity frame - Box sections (B×t)			
	E53° (DCR)	E69° (DCR)	E76° (DCR)	E79° (DCR)	Column (DCR)			
1	70×3.0 (0.82)	60×3.0 (0.85)	60×3.0 (0.97)	65×3.0 (0.99)	100×5.0 (0.98)			
2	70×3.0 (0.70)	55×2.5 (0.86)	55×2.5 (0.91)	55×2.5 (0.94)	85×5.0 (0.99)			
3	70×3.0 (0.59)	50×2.5 (0.82)	50×2.5 (0.82)	50×2.5 (0.82)	75×5.0 (0.90)			
4	55×2.5 (0.89)	50×2.5 (0.69)	45×2.0 (0.91)	45×2.0 (0.84)	65×4.5 (0.88)			
5	55×2.5 (0.81)	40×2.0 (0.93)	40×2.0 (0.82)	40×2.0 (0.53)	50×3.5 (0.98)			
6	55×2.5 (0.75)	40×2.0 (0.77)	35×1.5 (0.81)		40×3.0 (0.75)			
7	55×2.5 (0.69)	35×1.5 (0.96)						
8	55×2.5 (0.63)	30×1.5 (0.91)						
9	55×2.5 (0.57)	30×1.5 (0.61)						
10	45×2.0 (0.79)							
11	45×2.0 (0.71)							
12	45×2.0 (0.63)							
13	40×2.0 (0.61)							
14	40×2.0 (0.51)							
15	40×2.0 (0.43)							
16	30×1.5 (0.61)							
17	30×1.5 (0.49)							
18	30×1.5 (0.31)							

Module	E53°I53°		E69°I53°		E76°I53°		E79°I53°	
	I53° (DCR)	E53° (DCR)	I53° (DCR)	E69° (DCR)	I53° (DCR)	E76° (DCR)	I53° (DCR)	E79° (DCR)
1	95×4.5 (0.76)	70×3.0 (0.76)	95×4.5 (0.85)	60×3.0 (0.72)	100×4.5 (0.91)	60×3.0 (0.71)	100×4.5 (0.96)	60×3.0 (0.72)
2	95×4.5 (0.71)	70×3.0 (0.69)	95×4.5 (0.74)	55×2.5 (0.82)	100×4.5 (0.79)	55×2.5 (0.78)	100×4.5 (0.85)	55×2.5 (0.78)
3	95×4.5 (0.65)	70×3.0 (0.65)	95×4.5 (0.66)	50×2.5 (0.79)	100×4.5 (0.69)	50×2.5 (0.74)	100×4.5 (0.73)	50×2.5 (0.72)
4	85×4.0 (0.75)	55×2.5 (0.89)	85×4.0 (0.74)	50×2.5 (0.68)	85×4.0 (0.76)	40×2.0 (0.89)	85×4.0 (0.81)	40×2.0 (0.78)
5	85×4.0 (0.70)	55×2.5 (0.81)	85×4.0 (0.69)	40×2.0 (0.88)	85×4.0 (0.70)	35×1.5 (0.99)	85×4.0 (0.71)	30×1.5 (0.71)
6	85×4.0 (0.65)	55×2.5 (0.75)	85×4.0 (0.62)	40×2.0 (0.76)	85×4.0 (0.65)	30×1.5 (0.86)	85×4.0 (0.67)	
7	70×3.5 (0.82)	55×2.5 (0.96)	70×3.5 (0.81)	35×1.5 (0.89)	70×3.5 (0.82)		70×3.5 (0.83)	
8	70×3.5 (0.75)	55×2.5 (0.63)	70×3.5 (0.71)	30×1.5 (0.83)	70×3.5 (0.75)		70×3.5 (0.76)	
9	70×3.5 (0.69)	55×2.5 (0.58)	70×3.5 (0.65)	30×1.5 (0.57)	70×3.5 (0.69)		70×3.5 (0.69)	
10	60×3.0 (0.83)	45×2.0 (0.75)	60×3.0 (0.79)		60×3.0 (0.85)		60×3.0 (0.84)	
11	60×3.0 (0.74)	45×2.0 (0.71)	60×3.0 (0.74)		60×3.0 (0.76)		60×3.0 (0.76)	
12	60×3.0 (0.65)	45×2.0 (0.63)	60×3.0 (0.65)		60×3.0 (0.68)		60×3.0 (0.68)	
13	55×2.5 (0.73)	40×2.0 (0.62)	50×2.5 (0.81)		50×2.5 (0.85)		50×2.5 (0.86)	
14	55×2.5 (0.61)	40×2.0 (0.52)	50×2.5 (0.68)		50×2.5 (0.72)		50×2.5 (0.73)	
15	55×2.5 (0.49)	40×2.0 (0.44)	50×2.5 (0.55)		50×2.5 (0.59)		50×2.5 (0.62)	
16	40×2.0 (0.69)	30×1.5 (0.65)	40×2.0 (0.69)		40×2.0 (0.74)		40×2.0 (0.76)	
17	40×2.0 (0.48)	30×1.5 (0.49)	40×2.0 (0.48)		40×2.0 (0.53)		40×2.0 (0.55)	
18	40×2.0 (0.31)	30×1.5 (0.34)	40×2.0 (0.31)		40×2.0 (0.35)		40×2.0 (0.35)	

4. Weight of consumed steel materials and structures' stiffness

The amount of steel material consumption in structural systems is an important factor to choose an economical system. The total weight of steel materials in archetypes considering the variation of exterior and interior configuration are provided in Fig. 5(a). This weight is comprised of interior and exterior steel frames weight in addition to gravity beams. The structural weight of different diagrid archetypes are calculated between 0.62-0.84 KN/m^2 which is quite less than the presented value of 1.43 KN/m^2 for tall buildings constructed in high-seismic zone

(Taranath 2012). It can be observed that the exterior diagonal angles with different configurations of interior frames have a significant effect on the usage of steel materials. The lowest steel material is used for E69° model compared to other diagrid archetypes with interior gravity frame. In the external diagonal angle of E53°, bending rigidity of system decreases and then larger cross-sections are needed for diagonals to carry gravity loads. On the other hand, for steeper diagonal angle (E79°), larger cross-sections are needed for diagonals to compensate for the lack of shear rigidity. In the case of E76° and E79° models with different internal tubes, the weight of steel material are 5% and 12% heavier than E69° model, respectively. In addition, Exterior tube with diagonal angle of 53° coupled with

Table 3 Results of modal analysis

Performance group	Archetype ID	Transitional Modes (s)			Torsional Modes (s)	
		1 st	2nd	3rd	1st	2nd
PG-1	E53°	2.94	0.74	0.32	0.78	0.30
	E69°	3.20	1.03	0.57	1.34	0.53
	E76°	3.72	1.26	0.73	1.81	0.83
	E79°	4.24	1.46	0.86	2.25	0.83
PG-2	E53°I53°	2.89	0.73	0.49	0.76	0.6
	E69°I53°	3.02	0.92	0.48	1.23	0.49
	E76°I53°	3.41	1.09	0.60	1.56	0.63
	E79°I53°	3.66	1.16	0.62	1.76	0.68
PG-3	E53°I69°	2.85	0.74	0.50	0.80	0.50
	E69°I69°	3.05	0.96	0.54	1.34	0.54
	E76°I69°	3.37	1.11	0.62	1.76	0.68
	E79°I69°	3.98	1.23	0.68	2.08	0.80
PG-4	E53°I76°	2.88	0.76	0.50	0.80	0.56
	E69°I76°	3.09	0.98	0.54	1.36	0.56
	E76°I76°	3.44	1.13	0.65	1.77	0.70
	E79°I76°	3.95	1.28	0.74	2.22	0.85
PG-5	E53°I79°	2.89	0.77	0.55	0.81	0.50
	E69°I79°	3.07	0.98	0.55	1.30	0.54
	E76°I79°	3.46	1.16	0.67	1.80	0.70
	E79°I79°	3.87	1.31	0.77	2.18	0.86

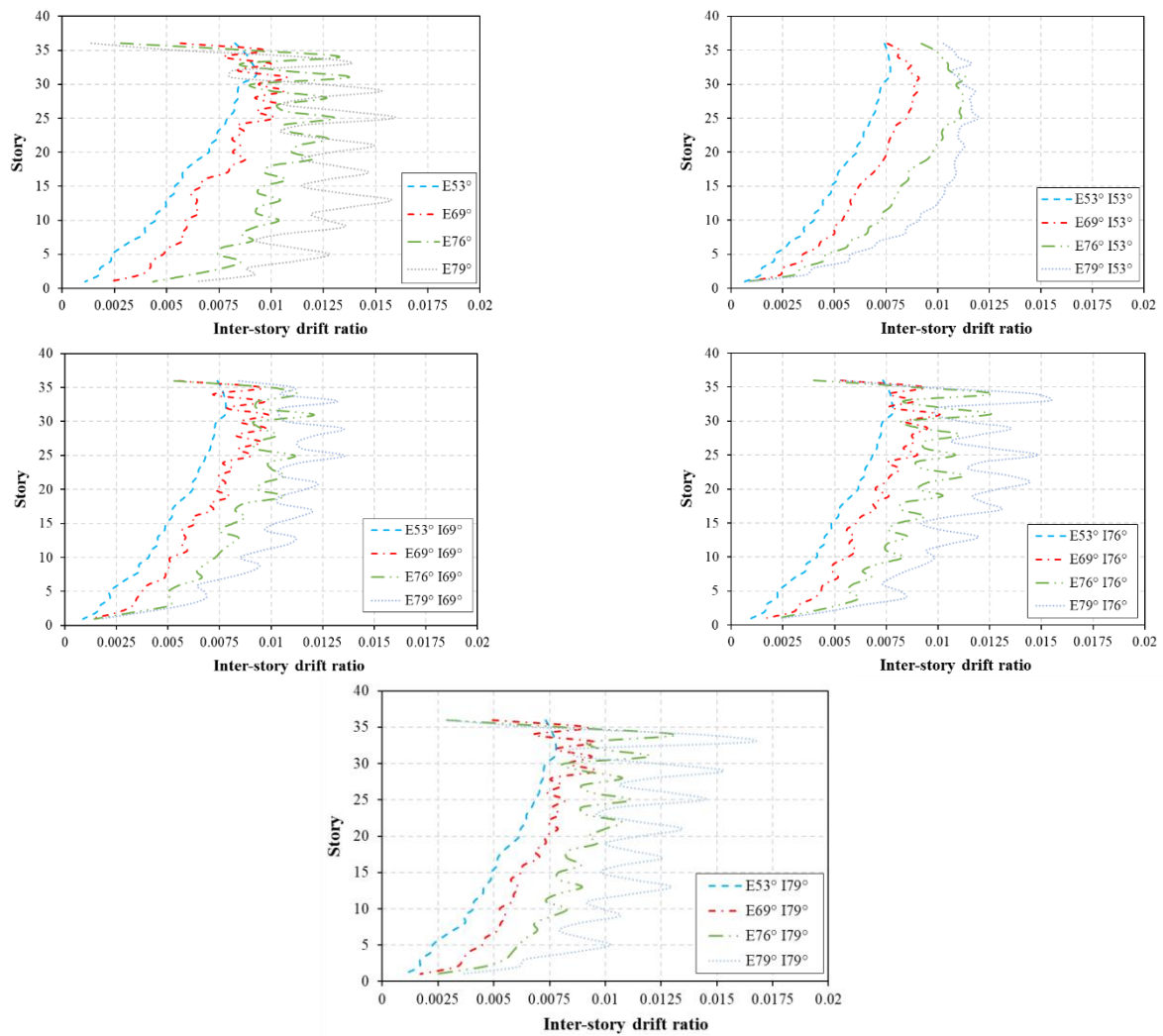


Fig. 4 Inter-story drift ratio of diagrid archetypes

interior diagrid tube including diagonal angle of 69°-79° (E53°I69°- E53°I79°) are approximately 20% heavier than those of E69°I69°- E69°I79° models.

According to Fig. 5(a), the diagonal angle of 69°-79° for diagrid core leads to the smallest amount of consumed steel material compared to models with I53°. The reason is that in the considered plan layout, about 45% of gravity loads are carried by the core system and the efficient diagonal angle of core increases to resist gravity loads as well as lateral loads. Therefore, the diagonal angle of 69°, 76° and 79° for diagrid core with the external frame slope of 69° are the most efficient angles to carry gravity and lateral loads. Finally, it can be seen that the variations of steel consumption highly depend on the diagonal angle of exterior diagrid.

Lateral stiffness of typical diagrid and tube-in-tube diagrid buildings are compared in Fig. 5(b). In tube-in-tube diagrid buildings that include a diagrid core for resisting lateral loads, the lateral stiffness increases up to 45% compared to typical diagrid buildings. However, Moon *et al.* (2007) concluded that adding a braced core to diagrid buildings provided only 1/5 of the total stiffness provided by the perimeter diagrid. This can imply high potential of diagrid core in providing additional stiffness to the structure by consumption of equal materials compared to typical diagrid structures.

5. Nonlinear analyses

5.1 Nonlinear modeling

The 3-Dimensional finite element modeling of the structures have been created in PERFORM-3D software due to its capability to model nonlinear behavior of structural members using fiber sections (Perform-3D). In tall diagrid structures inclined members play an important role in absorbing and dissipating energy as a result of induced motions in earthquakes. Hence, nonlinear modeling must include all sources of cyclic deteriorations in members affecting resulting response. In this regard, the numerical model of braces are employed completely in accordance with ASCE41 based on members' compactness (ASCE 2013). In addition, all inclined members are modeled with fiber sections on the basis of inelastic buckling and yielding properties of steel fiber segments. The typical stress-strain relationship of steel section is illustrated in Fig. 6(a). In this figure ϵ is the longitude deformation of brace. ϵ_x is related to the point corresponded to the residual strength and ϵ_u is the ultimate deformation of material which causes collapse. numerical modeling in OpenSees (Heshmati and Aghakouchak 2018). As shown in Fig. 7, numerical modeling of diagonals in this study are in a good agreement with numerical simulation in OpenSees (Heshmati and Aghakouchak 2018) and Black *et al.*'s experimental test (1980).

5.2 Nonlinear static analyses

Nonlinear static analysis has been widely used in previous studies in order to estimate the behavior of

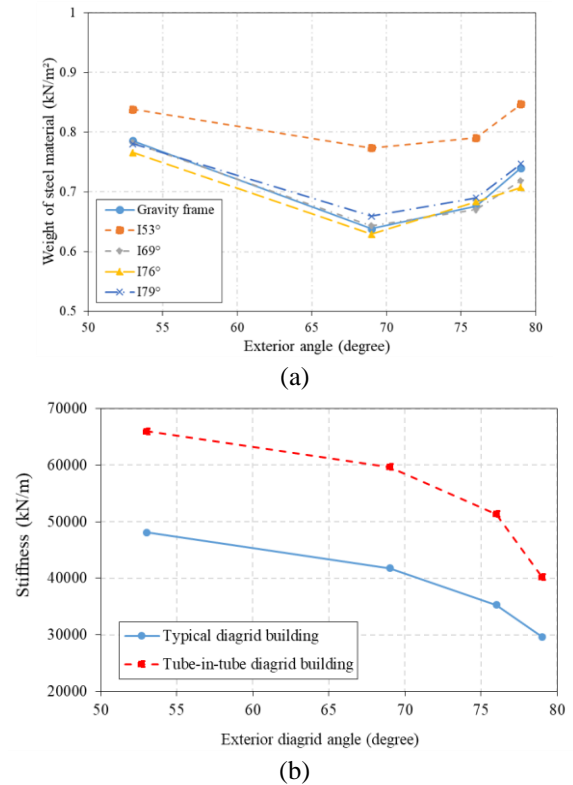


Fig. 5 (a) Unit weight of steel consumed in different archetypes (b) Stiffness of typical and corresponding average values for tube-in-tube diagrid buildings

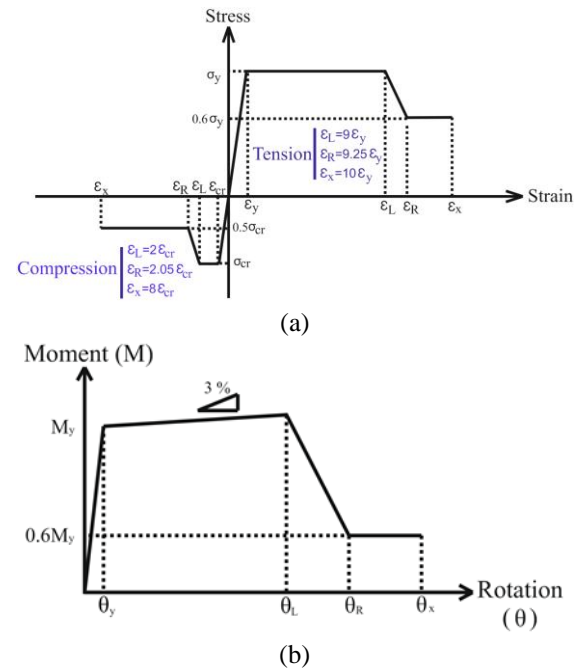
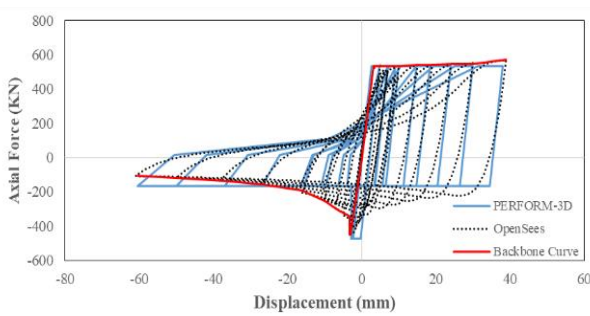


Fig. 6 (a) Stress-strain constitutive model of fiber segments for steel diagonal members (b) Moment-Rotation relationship of steel beams

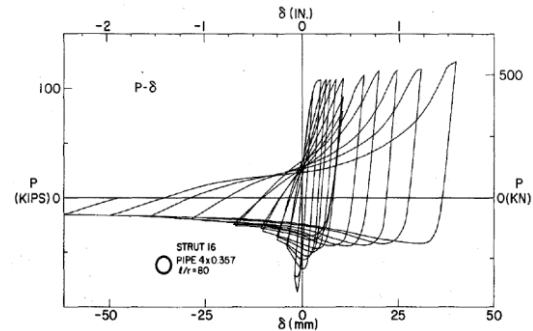
structures subjected to seismic events (Trabelsi *et al.* (2017), Hashemi *et al.* (2017), Veismoradi and Darvishan (2018)). In this study, nonlinear static analyses were

Table 4 Results of nonlinear static analyses

Performance group	Archetype ID	T_1 (sec)	V_d (kN)	V_{max} (kN)	$\delta_{y,eff}$ (m)	δ_u (m)	μ_T	Average of μ_T	Ω	Average of Ω
PG-1	E53°	2.94	25008	68447.46	0.62	1.20	1.94	1.96	2.74	2.05
	E69°	3.20	24575	54647.52	0.59	1.20	2.03		2.22	
	E76°	3.72	24698	40434.22	0.59	1.50	2.54		1.64	
	E79°	4.24	24912	39633.09	0.75	1.02	1.36		1.59	
PG-2	E53°I53°	2.89	25400	81178.96	0.70	3.14	4.48	4.46	3.20	2.55
	E69°I53°	3.02	24731	66295.82	0.64	1.27	1.99		2.68	
	E76°I53°	3.41	25297	53258.09	0.64	4.00	6.25		2.11	
	E79°I53°	3.66	25267	56434.04	0.78	4.00	5.12		2.23	
PG-3	E53°I69°	2.85	25973	77851.96	0.64	3.50	5.48	3.63	3.00	2.30
	E69°I69°	3.05	25428	58950.17	0.56	2.00	3.57		2.32	
	E76°I69°	3.37	25180	57812.02	0.71	2.50	3.52		2.30	
	E79°I69°	3.98	25793	40107.17	0.63	1.25	1.99		1.61	
PG-4	E53°I76°	2.88	25856	75816.83	0.63	3.30	5.23	3.16	2.93	2.51
	E69°I76°	3.09	25197	68472.05	0.66	2.00	3.03		2.72	
	E76°I76°	3.44	25613	61395.90	0.73	2.20	3.01		2.40	
	E79°I76°	3.95	25928	51602.96	0.81	1.10	1.36		1.99	
PG-5	E53°I79°	2.89	25804	74679.24	0.62	3.30	5.32	2.45	2.89	2.54
	E69°I79°	3.07	25264	62242.86	0.59	1.80	3.05		2.46	
	E76°I79°	3.46	25050	61711.36	0.74	2.10	2.84		2.46	
	E79°I79°	3.87	26169	61564.54	0.92	2.60	2.83		2.35	



(a)



(b)

Fig. 7 (a) Hysteretic response of the numerical model in Perform3D and a validated analytical OpenSees model (Heshmati and Aghakouchak 2018) (b) Hysteretic response of experimental test (Black et al. 1980)

performed based on the FEMA P695 methodology to determine two seismic performance factors including over-strength factor (Ω) and period-based ductility factor (μ_T). Lateral load is distributed along the height of structures based on the fundamental mode shape. The gravity load combination was imposed on the archetypes as

$$\text{Gravity Load} = 1.05\text{Dead Load} + 0.25\text{Live Load} \quad (5)$$

Pushover curves of both tube-in-tube and typical diagrid buildings are plotted in Fig. 8. Buckling of diagonal members lead to sequential drops in pushover curves showing load redistribution capacity of diagrid systems that provide adequate resistance against lateral loads. Buckling of diagonal members occurs when axial force exceeds the compressive strength according to chapter E of AISC360-16 (ANSI 2016). The results of nonlinear static analyses are summarized in Table 4 for all archetypes in different performance groups. The over-strength factor (Ω) are calculated as

$$\Omega = \frac{V_{max}}{V_d} \quad (6)$$

Where V_{max} and V_d are the maximum base shear capacity and design base shear, respectively. The period-based ductility factor (μ_T) is calculated as the ratio of ultimate roof displacement, δ_u , to the effective yield roof displacement, $\delta_{y,eff}$, as follows

$$\mu_T = \frac{\delta_u}{\delta_{y,eff}} \quad (7)$$

The maximum roof displacement, δ_u , is defined as the roof displacement in which a drop of 20% of the maximum base shear capacity is observed (FEMA P695 June 2009). The parameter $\delta_{y,eff}$ is calculated as

$$\delta_{y,eff} = C_0 \frac{V_{max}}{W} \left(\frac{g}{4\pi^2} \right) (\max(T, T_1))^2 \quad (8)$$

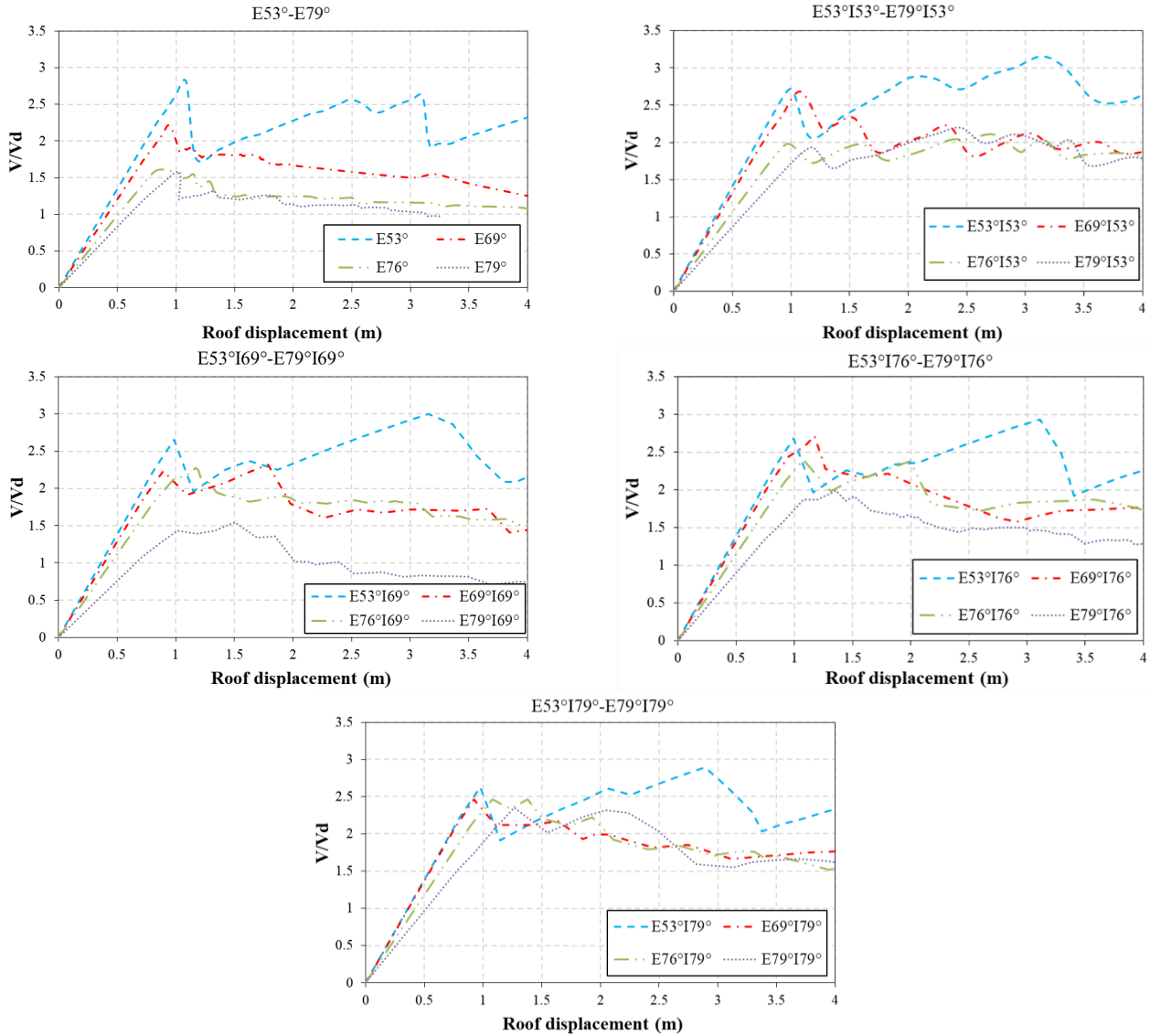


Fig. 8 The pushover curves of diagrid archetypes

In which, W is the building weight, g is the gravity constant, T is the approximate fundamental period obtained using Section 5.2.5 of the FEMA P695, T_1 is the analytical fundamental period calculated using the eigenvalue analysis. Also the coefficient C_0 relates fundamental-mode (SDOF) displacement to roof displacement of multiple degree of freedom (MDOF) and is calculated as

$$C_0 = \phi_{1,r} \frac{\sum_1^N m_x \phi_{1,x}}{\sum_1^N m_x \phi_{1,x}^2} \quad (9)$$

Where m_x is the mass at level x , and $\phi_{1,x}$ ($\phi_{1,r}$) is the ordinate of the fundamental mode at level x (roof), and N is the number of levels.

According to Table 4, for archetypes E53° to E79°, over-strength factor decreases by increasing diagonal angle as their amounts dropped from 2.74 to 1.59, respectively. The over-strength factor increases as interior gravity frames were replaced with diagrid systems. It can be observed that core diagrid can increase the over-strength factor up to 50%

compared to those of typical diagrid models. This effect is more significant when the slope of exterior frame rises. The results also indicate that with the rise in the inclination of exterior tube, the over-strength factors decrease. The effects of interior diagrid core on the ductility of high-rise diagrid structures are noticeable, as it is indicated on average the ductility grows considerably when the interior frame is a diagrid core. On average PG-2 demonstrates the highest growth in the ductility factor and it reduces as the internal tube angle rises

The impacts of diagrid core and diagonal slope variations are indicated in Fig. 9. Buckling of diagonal members occurs when axial force exceeds the compressive strength according to chapter E of AISC360-16. Diagrid buildings consist of four orthogonal frames which are divided into three groups. The frames which are parallel to lateral loading are called web frames, and according to the direction of lateral loading those that are perpendicular to the loading are named either tensile or compressive flanges. Large axial forces are imposed to corner diagonals from

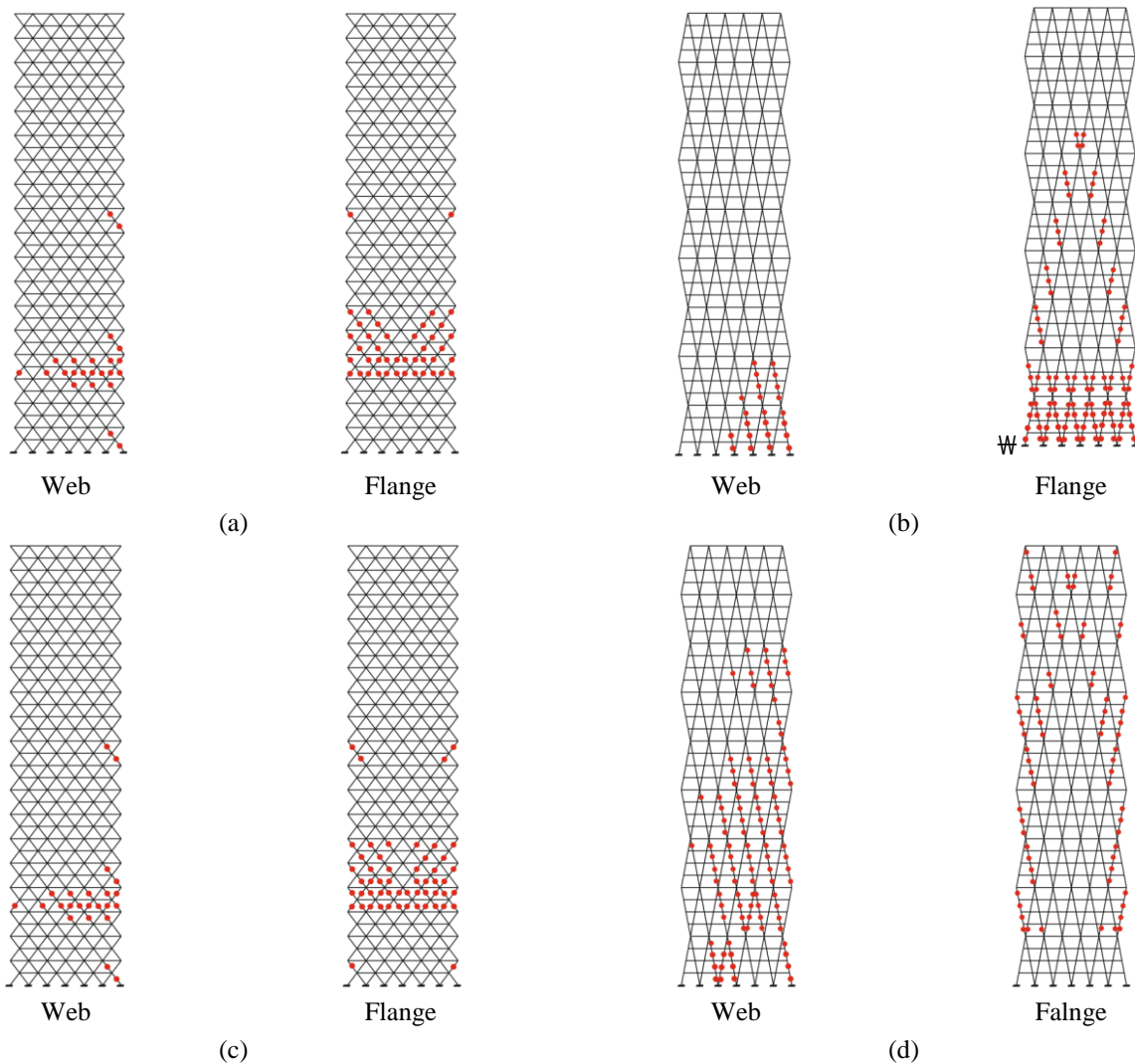


Fig. 9 Buckling members in (a) E53° (b) E79° (c) E53°I76° (d) E79°I76°

both web and flange frames, hence these elements are highly prone to buckling under lateral loading (Günel and Ilgin 2014) and as it can be observed in Fig. 1 (Fig. 9 in the revised manuscript), buckling initiates from corner diagonals.

Variations in diagonal angles lead to changes in distribution of buckling members and failure of the whole structure along the height of the building. For E53° diagrid building (Fig. 1(a)), buckled diagonal members were concentrated in a small number of stories at lower modules. This pattern usually occurs for diagrid structures with low diagonal slope and is very close to “Zipper-type” failure mode introduced by Starossek (2007, 2009), in which failure of one element and forces’ redistribution to adjacent bays resulted in failure of the whole structure and increased the probability of soft story occurrence. However, for archetypes with steeper diagonal slopes (Fig. 1(b)), the buckled members were distributed along the height of first module. Thus, the rapid instability and collapse of the structure could be procrastinated (Asadi and Adeli 2018) and the failure of structure is dependent on the failure of one module. Furthermore, by adding diagrid core to

buildings with low diagonal slope (Fig. 1(c)), sequence of buckling members remains fairly the same as typical diagrid buildings. But, it completely changes in buildings with steep diagonal slope (Fig. 1(d)). As it can be seen, buckling of members are well distributed between several modules along the height of tube-in-tube diagrid building compared to the typical diagrid structures, where the plastic hinges mostly spread in lower stories of the diagrid buildings (Kim and Lee 2012). Therefore, it allows the structure to experience large deformations before global collapse occurrence.

5.3 Incremental dynamic analyses and collapse fragility curves

Over the last years, Incremental Dynamic Analysis (IDA) and fragility analysis have been used in several studies in order to assess the capacity of different structural systems (Song and Guo 2017, Li *et al.* 2017, Beilic *et al.* 2017). Herein, Incremental dynamic analysis was performed to quantify the median collapse capacity (\hat{S}_{CT}) and collapse margin ratio (CMR) of each archetype based

Table 5 Far-field ground motion characteristics for IDA (FEMA P695 (June 2009))

ID No.	Name	Year	Magnitude	Station	Site class (NEHRP)	Fault type	PGA _{max} (g) *	PGV _{max} (cm/s) *
1	Northridge	1994	6.7	Beverly Hills	D	Thrust	0.52	63
2	Northridge	1994	6.7	Canyon Country-WLC	D	Thrust	0.48	45
3	Duzce, Turkey	1999	7.1	Bolu	D	Strike-slip	0.82	62
4	Hector Mine	1999	7.1	Hector	C	Strike-slip	0.34	42
5	Imperial valley	1979	6.5	El Centro array #11	D	Strike-slip	0.38	42
6	Kobe, Japan	1995	6.9	Nishi-Akashi	C	Strike-slip	0.51	37
7	Kocaeli, Turkey	1999	7.5	Duzce	D	Strike-slip	0.36	59
8	Manjil, Iran	1990	7.4	Abbar	C	Strike-slip	0.51	54
9	Superstition Hills	1987	6.5	El Centro Imp. Co. Cent	D	Strike-slip	0.36	46
10	San Fernando	1971	6.6	LA-Hollywood Stor FF	D	Thrust	0.21	19
11	Friuli, Italy	1976	6.5	Tolmezzo	C	Thrust	0.35	31

on the FEMA P695. Two sets of far-field (22 pairs of records) and near-field (28 pairs of records) ground motion records have been proposed in this methodology for IDA analysis. The records were scaled in two steps before they were used in IDA. First, individual records were normalized by their peak ground velocity to remove unwarranted variability between records. The frequency content of records was not changed during this procedure. Second, the normalized ground motion records were collectively scaled upward or downward to match the MCE spectral acceleration at the fundamental period of the archetype under consideration, T. The characteristics of input ground motions in this research are summarized in Table 5.

IDA was performed on the archetypes of PG-1 (E53°-E79°) and PG-3 (E53°I69°-E79°I69°) under ground motion records of Table 4. To compare the collapse capacity of tube-in-tube diagrids with typical diagrid buildings, diagrid core with angle of 69° (I69°) was selected as it is optimum configuration in terms of steel material consumption according to section 4 and it was indicated the lowest over-strength factor in pushover analyses, hence the outputs can be considered as conservative values. On average, 350 nonlinear time history analyses were conducted to develop IDA curves for each archetype. This analysis includes a number of time history analyses in which the ground motion intensity of the records is increased gradually until the collapse state of archetype is achieved. According to Vamvatsikos and Cornell, the determination of collapse point for stopping the analyses in IDA can be assumed as either of the intensity of the ground motions which result in the maximum inter-story drift of 10% or where the local tangent of IDA curve reaches 20% of the elastic slope, whichever achieves first (2002). The IDA curves for archetypes of PG-1 and PG-3 are illustrated in Fig. 10. The spectral intensity of the applied ground motion records as Intensity Measure (IM) are plotted versus maximum inter-story drift ratio as Engineering Demand (ED). According to Vamvatsikos and Cornell (2002a, 2002b), median IDA curves are considered to summarize and compare IDA curve sets. Median curves in Fig. 10 show that increasing exterior diagonal angle, resulted in increasing inter-story drift and

Table 6 Summary of collapse results for archetypes of PG-1 and PG-3

Performance group (PG)	Archetype ID	\hat{S}_{CT} [g]	CMR	SSF	ACMR
PG-1	E53°	1.10	3.49	1.23	4.29
	E69°	0.86	2.73	1.24	3.38
	E76°	0.63	2.00	1.29	2.58
	E79°	0.50	1.59	1.22	1.94
PG-3	E53°I69°	1.40	4.44	1.48	6.57
	E69°I69°	0.94	2.98	1.36	4.05
	E76°I69°	0.76	2.41	1.36	3.28
	E79°I69°	0.60	1.90	1.23	2.34

Table 7 Values of different uncertainties and total collapse uncertain

Archetype ID	μ_T	β_{RTR}	β_{DR}		β_{TD}		β_{MDL}		β_{TOT}
			Design qual ity= Good	Test data ality= Fair	qu	Modeling qu ality= Good	qu		
E53°	1.92	0.292	0.2	0.35	0.2	0.2	0.2	0.536	
E69°	1.73	0.273	0.2	0.35	0.2	0.2	0.2	0.526	
E76°	2.5	0.350	0.2	0.35	0.2	0.2	0.2	0.570	
E79°	1.84	0.284	0.2	0.35	0.2	0.2	0.2	0.532	
E53°I69°	1.95	0.295	0.2	0.35	0.2	0.2	0.2	0.538	
E69°I69°	1.66	0.266	0.2	0.35	0.2	0.2	0.2	0.523	
E76°I69°	1.47	0.247	0.2	0.35	0.2	0.2	0.2	0.513	
E79°I69°	1.36	0.236	0.2	0.35	0.2	0.2	0.2	0.508	

displacement demands for a same intensity measure. However, adding diagrid core leads to decreasing inter-story drift values and displacement demands for a same intensity measure.

The collapse fragility curves of archetypes are achieved by cumulative distribution function of collapse points from IDA results. This curve shows the probability of structural collapse for a specific ground motion intensity. Fig. 11 illustrates fragility curves for archetypes of PG1 and PG3. Then collapse margin ratio, CMR, of diagrid archetypes are determined to evaluate collapse safety of diagrid structures. According to Eq. 10, CMR is the ratio between the median collapse intensity, \hat{S}_{CT} , and the MCE intensity, S_{MT} . The calculated CMR values for diagrids are presented in Table

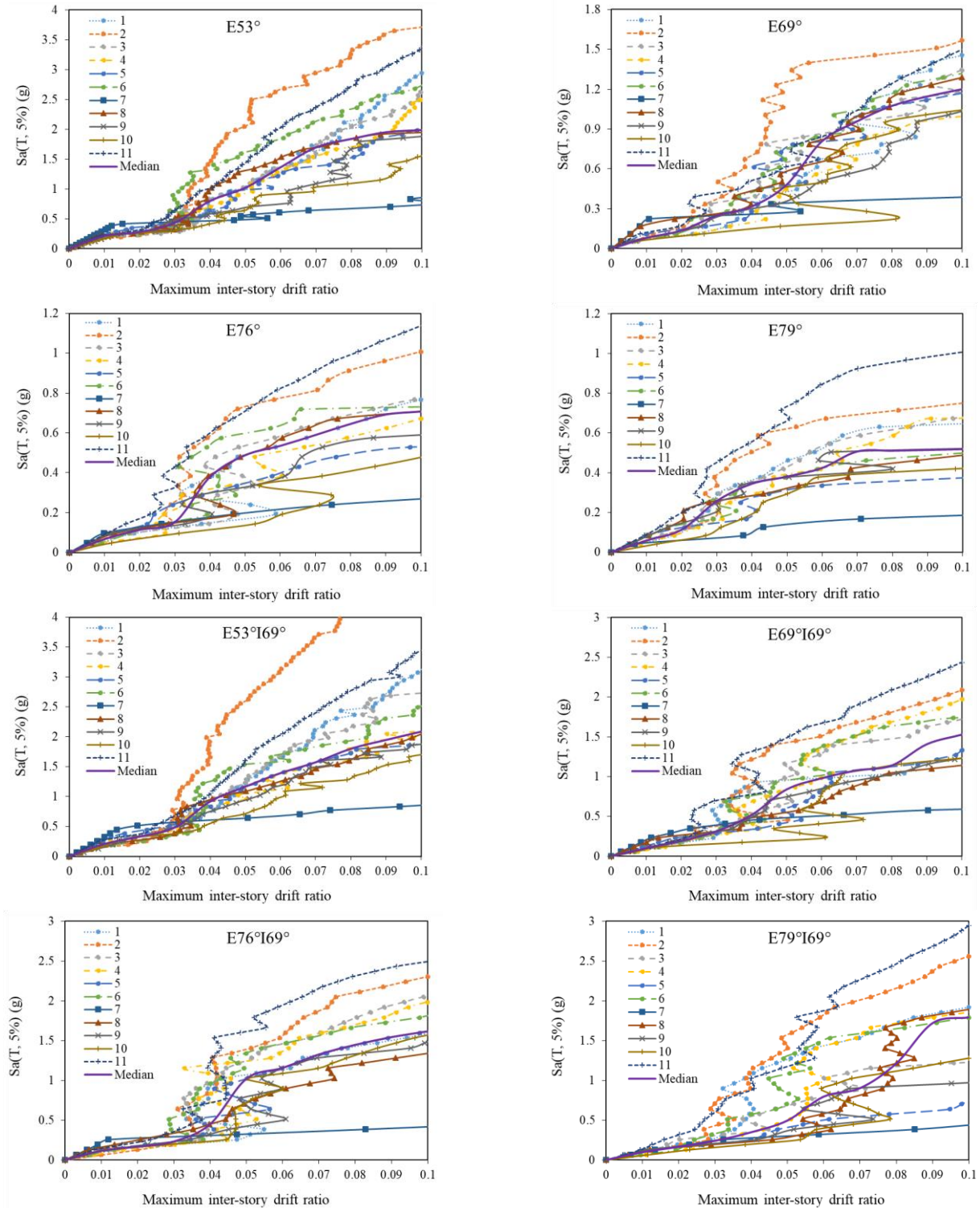


Fig. 10 Results of incremental dynamic analysis for archetypes of PG-1 and PG-3

5.

$$\text{CMR} = \frac{\hat{S}_{\text{CT}}}{S_{\text{MT}}} \quad (10)$$

Results from fragility curves in Fig. 11 indicate that the median collapse capacity of tube-in-tube diagrid buildings are larger than those of typical diagrid buildings. As well as this, in both typical diagrid buildings and tube-in-tube

diagrid buildings, as the diagonal slope of exterior tube decreases, collapse probability of archetypes also reduces.

It also can be seen that the collapse probability of archetypes under the MCE intensity S_{MT} for both with and without core groups are under 5% except for E79° and E79°I69° which are shown to be around 10%. It should be noted that the MCE intensity S_{MT} for all archetypes is equal to 0.31 g.

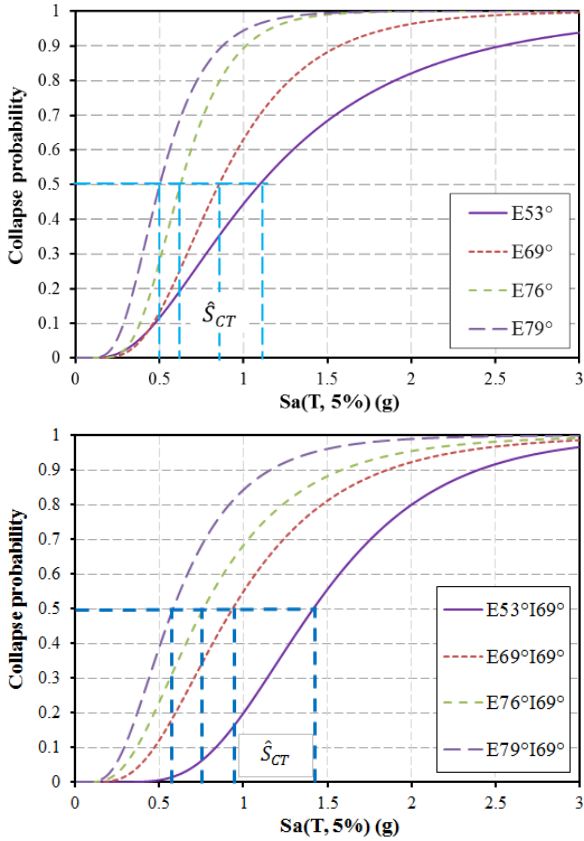


Fig. 11. Collapse fragility curves for archetypes of PG-1 and PG-3

According to FEMA P695 methodology and the data presented in Table 6, the collapse intensity (\hat{S}_{CT}) which causes 50% probability of collapse, is the basis for the calculation of collapse margin ratio (CMR) and these quantities are larger in core diagrid structures which contributed to higher CMR. This represents the fact that interior core diagrid provides sufficient resistance against collapse for diagrid buildings.

In the next step, calculated CMRs need to be modified by spectral shape factor, SSF which can be considered as an indicator of ductility in collapse resistance of archetypes under dynamic motions to obtain adjusted collapse margin ratio (ACMR) of each index archetypes. The SSF and ACMR of each archetype in PG-1 and PG-3 are presented in Table 6. All the calculated SSF values for each group are in the same order, however, tube-in-tube diagrid structures demonstrate a slight increase in the values which lead to larger quantities of ACMR. ACMR of each index archetype is calculated as follows

$$ACMR = SSF \times CMR \quad (11)$$

The spectral shape factor considers frequency content of the ground motion records which depends on the fundamental period of structure, T , the period based ductility, μ_T , and the seismic design category. The SSF is determined as follows

$$SSF = \exp[\beta_1 \times (\bar{\epsilon}_0(T) - \bar{\epsilon}^-(T)_{records})] \quad (12)$$

$$\beta_1 = (0.14)(\mu_T - 1)^{0.42} \leq 0.317 \quad , \quad 0 \leq \bar{\epsilon}^-(T)_{records} = (0.6)(1.5 - T) \leq 0.6$$

$$\bar{\epsilon}_0(T) = \begin{cases} 1.0 & \text{for SDC B and C} \\ 1.5 & \text{for SDC D} \\ 1.2 & \text{for SDC E} \end{cases} \quad (13)$$

Based on FEMA P695, β_1 depends on the building inelastic deformation capacity. $\bar{\epsilon}^-(T)_{records}$ is for the far-field record sets and $\bar{\epsilon}_0$ depends on the Seismic Design Category (SDC) from SDC B to SDC E indicating the lowest to highest seismicity, respectively (FEMA P695 June 2009).

During this procedure, different uncertainties influence the collapse capacity of structures. The sources of uncertainties in FEMA P695 include record-to-record (β_{RTR}) uncertainty, design requirement (β_{DR}) uncertainty, test data (β_{TD}) uncertainty, and modeling (β_{MDL}) uncertainty. The value of RTR uncertainty, β_{RTR} , accounts variability of ground motions which is related to the period-based ductility as follows

$$0.2 \leq \beta_{RTR} = 0.1 + 0.1\mu_T \leq 0.4 \quad (14)$$

According to FEMA P695 methodology, β_{DR} , β_{TD} and β_{MDL} are determined based on four levels of superior, good, fair, and poor with quantitative scales of 0.1, 0.2, 0.35 and 0.5, respectively. In addition, the total collapse uncertainty, β_{TOT} , is calculated as Eq. (15) assuming uncertainties to be independent.

$$\beta_{TOT} = \sqrt{\beta_{RTR}^2 + \beta_{DR}^2 + \beta_{TD}^2 + \beta_{MDL}^2} \quad (15)$$

The quantitative values of uncertainties and total collapse uncertainty for archetypes are presented in Table 7. In this study, we used Table D1.1 of ANSI/AISC 341 (ANSI 2016) to limit the diameter to thickness ratios of diagonals and ANSI/AISC 360-16 (ANSI 2016) to design diagonal members as tubular sections. In diagrid structures, the diagonals carry the vertical and horizontal loads through axial compression or tension forces. Also we used ANSI/AISC 360-16 (ANSI 2016) to design floor, ring beams and gravity columns. Therefore, due to the robustness and high confidence level of these design requirements, a quality rating of good equal to 0.2 was selected for design requirement uncertainty. Although there is no comprehensive experimental test investigating the behavior of diagrid frames under earthquake, a large number of analytical and experimental studies have been carried out to investigate individually the behavior of axially-loaded members, which are substantial elements in diagrids for carrying gravity and lateral loads. Therefore, test data uncertainty was supposed to be good equal to 0.35. Numerical models are developed three-dimensionally to consider the tubular behavior and accurately obtain the collapse capacity of archetypes through nonlinear analyses. In addition, the nonlinear models of members are adopted based on the force-deformation relationship of ASCE 41. The fiber section used for diagonal models captures global buckling, but are not capable to simulate local buckling behavior. As such, a quality rating of 0.35 was selected for

Table 8 Performance evaluation of diagrid archetypes according to FEMA P695

Archetype ID	Computed over-strength and adjusted collapse margin parameters		Acceptance control		
	Ω	ACMR	ACMR _{20%}	ACMR _{10%}	Pass/Fail
PG-1					
E53°	2.74	4.29	1.56	---	Pass
E69°	2.22	3.38	1.56	---	Pass
E76°	1.64	2.58	1.62	---	Pass
E79°	1.59	1.94	1.59	---	Pass
Average	2.05	3.05	---	2.02	Pass
PG-3					
E53°I69°	3.00	6.57	1.59	---	Pass
E69°I69°	2.32	4.05	1.59	---	Pass
E76°I69°	2.30	3.28	1.56	---	Pass
E79°I69°	1.61	2.34	1.56	---	Pass
Average	2.30	4.06	---	2.02	Pass

MDL uncertainty.

5.3.1 Quantification of response modification factor

To quantify the validity of presumed response modification factor, R , the calculated ACMR for each index archetype ($ACMR_i$) and the average value of ACMR for each performance group (\overline{ACMR}_i) must be greater than acceptable values of ACMR_{20%} and ACMR_{10%}, respectively. ACMR_{10%} and ACMR_{20%} are determined based on total collapse uncertainty from Table 7-3 of FEMA P695 (June 2009). According to Table 8, calculated values of $ACMR_i$ and \overline{ACMR}_i for both conventional diagrid and tube-in-tube diagrid buildings turned out to be greater than acceptable values of adjusted collapse margin ratio proposed by FEMA P695. Therefore, response modification factor equal to $R=3.0$ is valid for designing steel diagrid systems with 36-story. The adjusted collapse margin ratio for tube-in-tube diagrid buildings turned out to be larger than those of conventional diagrid buildings representing higher seismic safety margin for tube-in-tube diagrid buildings under severe earthquakes.

Asadi and Adeli (2018) proposed R factor in the range of 4 to 5 for 8- to 30-story conventional diagrid buildings. In addition, Heshmati and Aghakouchak (2018) recommended $R=4.5$ for the design of steel diagrid buildings up to 24-story based on FEMA P695 approach. Also Kim *et al.* (2010) performed three experimental tests on two-story scaled diagrid specimens and recommended $R = 4.97, 5.53, \text{ and } 5.86$ based on pushover curves. The proposed response modification factor equal to 3.0 in this research can be valid for tall tube-in-tube diagrid buildings.

5.3.2 Quantification of over-strength factor

According to FEMA P695, the largest value of over-strength factor among performance groups should be considered as system over-strength factor, Ω_0 . According to Table 7, for typical diagrid and tube-in-tube diagrid, the system over-strength factor is 2.05 and 2.29, respectively. These values need to be rounded to half unit intervals based on FEMA P695 methodology, hence $\Omega_0=2.0$ and $\Omega_0=2.5$ are presented for typical diagrid and tube-in-tube diagrid, respectively. Despite the over-strength factor of 3.0 recommended by researchers (Asadi and Adeli 2018, Heshmati and Aghakouchak 2018, Sadeghi and Rofooei 2018) for mid-rise diagrid buildings, the above mentioned

values would be practical for tall diagrid buildings.

6. Conclusions

In this study a new form of diagrid structures called tube-in-tube diagrid was introduced and the effects of changes in the angle of interior and exterior diagrid tube were investigated in detail on the seismic behavior of archetypes. Furthermore, the seismic performance factors e.g., ductility, over-strength and response modification factors were derived and compared with those of typical diagrid structures. Collapse probability of proposed models with various orientations in internal and external diagrid tube were examined thoroughly in both typical and tube-in-tube diagrid structures. Finally, proper response modification factor and over-strength factor were proposed for conventional and tube-in-tube diagrid buildings. Following conclusions are drawn from this study:

- The weight of structural steel elements in diagrid structures can be reduced to approximately half of the typical constructed tall buildings in seismic zones. In typical diagrid buildings, the diagonal angle of 69° for the exterior frame was the optimum angle in terms of steel material consumptions. This is also true for the angle of external tube in core diagrid structures. Also diagonal angle in the range of 69° to 79° for interior diagrid frame provided great reduction in the weight of tube-in-tube structures.
- Results of pushover analyses indicated that diagrid core can increase the over-strength factor up to 50% especially when the exterior frame angles are around 76°-79°. It was also evident that as the slope of exterior diagrid rose, the over-strength factor decreased.
- On average, interior diagrid frame had a notable impact on the ductility of typical diagrid structures, however, it reduced as the angle of diagonal members in core increased.
- According to the results of consumed steel materials and pushover analyses, E69°I69° and E69°I76° are recognized as the most favorable structural configurations in tall steel diagrid buildings in terms of cost efficiency, ductility and over-strength factor.
- Results from collapse fragility curves demonstrated that the median collapse capacity of tube-in-tube diagrid

buildings were larger than that of typical diagrid buildings. As well as this, in both typical diagrid buildings and tube-in-tube diagrid buildings, as the diagonal slope of exterior tube decreased, collapse probability of archetypes also reduced.

- The collapse probabilities of the archetypes corresponding to the spectral acceleration (S_{MT}) were less than 10%, representing the fact that both structural systems were safe under MCE ground motions.

- The Collapse Margin Ratio (CMR) and Adjusted Collapse Margin Ratio (ACMR) of tube-in-tube diagrid buildings were higher than those of typical diagrid buildings due to higher collapse capacity and ductility of core diagrid systems. It confirms high seismic safety margin of tube-in-tube diagrid buildings under severe excitations.

- The response modification factor of 3.0 was acceptable for the design of diagrid structures to achieve collapse criteria of FEMA P695. Furthermore, over-strength factors equal to $\Omega_0=2.0$ and $\Omega_0=2.5$ were suggested for typical diagrid structures and tube-in-tube diagrid structures, respectively.

- Finally, it was shown that not only the tube-in-tube diagrid can be constructed with the same consumed steel as was used in typical diagrid structures, but also it can significantly increase the over-strength factor and collapse capacity compared to typical diagrid building. In other words, in lieu of typical diagrid structures with conventional interior gravity frame, it is highly recommended to implement diagrid core in construction of high-rise buildings.

This study has been carried out to add diagrid cores to diagrid buildings and propose tube-in-tube diagrid building as an innovative structural system. In addition, seismic performance of typical diagrid and tube-in-tube diagrid buildings with various diagonal angles of interior and exterior frames were investigated thoroughly. Analysis results and the seismic performance factors are strictly valid for the range of parameters considered in this study. However, further studies for considering the effects of tributary areas of the interior and exterior frames are suggested.

References

- Al-Kodmany, K. and Ali, M.M. (2016), "An Overview of Structural and Aesthetic Developments in Tall Buildings Using Exterior Bracing and Diagrid Systems", *Int. J. High-Rise Build.*, **5**(4), 271-291. <https://doi.org/10.21022/ijhrb.2016.5.4.271>.
- Ali, M.M. and Moon, K.S. (2011), "Structural developments in tall buildings: Current trends and future prospects", *Architect. Sci. Rev.*, **50**(3), 205-223. <https://doi.org/10.3763/asre.2007.5027>.
- ANSI, A. (2016), *AISC 341-16: Seismic Provisions for Structural Steel Buildings*, Chicago, Illinois, USA: American Institute of Steel Construction (AISC).
- ANSI, A. (2016), *AISC 360-16*, Specification for Structural Steel Buildings.
- ANSI/AISC 341-10 (2010), *Seismic Provisions for Structural Steel Buildings*, American Institute of Steel Construction. Chicago, IL.
- Asadi, E. and Adeli, H. (2017), "Diagrid: An innovative, sustainable, and efficient structural system", *Struct. Des. Tall Spec. Build.*, **26**(8). <https://doi.org/10.1002/tal.1358>.
- Asadi, E. and Adeli, H. (2018), "Nonlinear behavior and design of mid-to high-rise diagrid structures in seismic regions", *Eng. J. Amer. Institute Steel Construct.*, **55**(3), 161-180.
- Asadi, E., Li, Y. and Heo, Y. (2018), "Seismic performance assessment and loss estimation of steel diagrid structures", *J. Struct. Eng.*, **144**(10), 04018179. [https://doi.org/10.1061/\(asce\)st.1943-541x.0002164](https://doi.org/10.1061/(asce)st.1943-541x.0002164).
- ASCE (2013), "ASCE/SEI 41-13: Seismic evaluation and retrofit of existing buildings".
- ASCE/SEI 7-16 (2016), *Minimum Design Loads for Buildings and Other Structures*, American Society of Civil Engineering.
- ATC-19 (1995), *Structural response modification factors*, Applied Technology Council, Redwood City, California.
- ATC-34 (1995), *A critical review of current approaches to earthquakeresistant design*, Applied Technology Council, Redwood City, California.
- ATC3-06 (1978), *Tentative provisions for the development of seismic regulations for buildings*, Applied Technology Council, Redwood City, California.
- Baker, W., Besjak, C., Sarkisian, M., Lee, P. and Doo, C.S. (2010), "Proposed methodology to determine seismic performance factors for steel diagrid framed systems", *Council Tall Build. Urban Habitat*.
- Beilic, D., Casotto, C., Nascimbene, R., Cicola, D. and Rodrigues, D. (2017), "Seismic fragility curves of single storey RC precast structures by comparing different Italian codes", *Earthq. Struct.*, **12**(3), 359-374. <https://doi.org/10.12989/eas.2017.12.3.359>.
- Black, K.G., Wenger, W.A. and Popov, E.P. (1980), *Inelastic Buckling of Steel Struts Under Cyclic Load Reversal*, Report 80/40. Earthquake Engineering Research center, University of California, Berkeley.
- Boake, T.M. (2014), *Diagrid structures: systems, connections, details*, Walter de Gruyter.
- Boake, T.M. (2016), "The Emergence of the Diagrid - It's All About the Node", *Int. J. High-Rise Build.*, **5**(4), 293-304. <https://doi.org/10.21022/ijhrb.2016.5.4.293>.
- Cina. Ministry of Construction of the People (2001), Code for seismic design of buildings. China Architecture & Building Press.
- Code, U.B. (1997), International Conference of Building Officials, Uniform Building Code, Whittier, California.
- Council, I.C. (2015), *2015 IBC: International Building Code*, ICC, International Code Council, Incorporated.
- CSI (Computers and Structures, Inc.) (2006), *Perform 3D, Nonlinear Analysis and Performance Assessment for 3D Structures User Guide*, Version 4.
- Farahi, M. and Mofid, M. (2013), "On the quantification of seismic performance factors of Chevron Knee Bracings, in steel structures", *Eng. Struct.*, **46**, 155-164. <https://doi.org/10.1016/j.engstruct.2012.06.026>.
- FEMA P695 (2009), *Quantification of building seismic performance factors*, Federal Emergency Management Agency, Washington, D.C.
- Freeman, S.A. (1990), "On the correlation of code forces to earthquake demands", *Proceedings of Fourth US-Japan Workshop on Improvement of Building Structural Design and Construction Practices*.
- Gade, V.P. and Sahoo, D.R. (2016), "Evaluation of collapse-resistance of special truss moment frames as per FEMA p695 approach", *Eng. Struct.*, **126**, 505-515. [doi:https://doi.org/10.1016/j.engstruct.2016.08.015](https://doi.org/10.1016/j.engstruct.2016.08.015).
- Günel, M.H. and Ilgin, H.E. (2014), *Tall buildings: structural systems and aerodynamic form*, Routledge.
- Hashemi, S.S., Sadeghi, K., Vaghefi, M. and Shayan, K. (2017), "Evaluation of ductility and response modification factor in

- moment-resisting steel frames with CFT columns”, *Earthq. Struct.*, **12**(6), 643-652. doi:https://doi.org/10.12989/eas.2017.12.6.643.
- Heshmati, M. and Aghakouchak, A.A. (2018), “Quantification of seismic performance factors of steel diagrid system”, *Struct. Des. Tall Spec. Build.*, **28**(3), e1572. doi:https://doi.org/10.1002/tal.1572.
- Heshmati, M., Khatami, A. and Shakib, H. (2020), “Seismic performance assessment of tubular diagrid structures with varying angles in tall steel buildings”, *Struct.*, **25**, 113-126. https://doi.org/10.1016/j.istruc.2020.02.030.
- Kamaludin, P.N.C., Kassem, M.M., Farsangi, E.N., Nazri, F.M. and Yamaguchi, E. (2020), “Seismic resilience evaluation of RC-MRFs equipped with passive damping devices”, *Earthq. Struct.*, **18**(3), 391-405. doi:https://doi.org/10.12989/eas.2020.18.3.391.
- Kheyroddin, A. and Mashhadiali, N. (2018), “Response modification factor of concentrically braced frames with hexagonal pattern of braces”, *J. Construct. Steel Res.*, **148**, 658-668. https://doi.org/10.1016/j.jcsr.2018.06.024.
- Kim, J. and Kong, J. (2012), “Progressive collapse behavior of rotor-type diagrid buildings”, *Struct. Des. Tall Spec. Build.*, **22**(16), https://doi.org/10.1002/tal.762.
- Kim, J. and Lee, Y.H. (2012), “Seismic performance evaluation of diagrid system buildings”, *Struct. Des. Tall Spec. Build.*, **21**(10), 736-749. https://doi.org/10.1002/tal.643.
- Kim, J., Park, J., Shin, S.W. and Min, K.W. (2009), “Seismic performance of tubular structures with buckling restrained braces”, *Struct. Des. Tall Spec. Build.*, **18**(4), 351-370. doi:https://doi.org/10.1002/tal.420.
- Kim, Y.J., Jung, I.Y., Ju, Y.K., Park, S.J. and Kim, S.D. (2010), “Cyclic behavior of diagrid nodes with H-section braces”, *J. Struct. Eng.*, **136**(9), 1111-1122. https://doi.org/10.1061/(asce)st.1943-541x.0000203.
- Kwon, K. and Kim, J. (2014), “Progressive collapse and seismic performance of twisted diagrid buildings”, *Int. J. High-Rise Build.*, **3**(3), 223-230. doi:https://doi.org/10.21022/IJHRB.2014.3.3.223.
- Leonard, J. (2007), *Investigation of shear lag effect in high-rise buildings with diagrid system*, Ph.D. Dissertation, Massachusetts Institute of Technology.
- Li, T., Yang, T.Y. and Tong, G. (2019), “Performance-based plastic design and collapse assessment of diagrid structure fused with shear link”, *Struct. Des. Tall Spec. Build.*, **28**(6), e1589. https://doi.org/10.1002/tal.1589.
- Li, Z., He, M., Lam, F., Zhou, R. and Li, M. (2017), “Seismic reliability evaluation of steel-timber hybrid shear wall systems”, *Earthq. Struct.*, **13**(3), 289-297. doi:https://doi.org/10.12989/eas.2017.13.3.289.
- Liu, C., Li, Q., Lu, Z. and Wu, H. (2018), “A review of the diagrid structural system for tall buildings”, *Struct. Des. Tall Spec. Build.*, **27**(4), https://doi.org/10.1002/tal.1445.
- Milana, G., Olmati, P., Gkoumas, K. and Bontempi, F. (2015), “Ultimate capacity of diagrid systems for tall buildings in nominal configuration and damaged state”, *Periodica Polytechnica Civil Eng.*, **59**(3), 381-391. https://doi.org/10.3311/PPci.7795.
- Miranda, E. and Bertero, V.V. (1994), “Evaluation of strength reduction factors for earthquake-resistant design”, *Earthq. Spectra*, **10**(2), 357-379. doi:https://doi.org/10.1193%2F1.1585778.
- Moghaddasi B.N.S. and Zhang, Y. (2013), “Seismic analysis of diagrid structural frames with shear-link fuse devices”, *Earthq. Eng. Vib.*, **12**(3), 463-472. doi:https://doi.org/10.1007/s11803-013-0186-9.
- Montuori, G.M., Mele, E., Brandonisio, G. and De Luca, A. (2014), “Design criteria for diagrid tall buildings: Stiffness versus strength”, *Struct. Des. Tall Spec. Build.*, **23**(17), 1294-1314. doi:https://doi.org/10.1002/tal.1144.
- Montuori, G.M., Mele, E., Brandonisio, G. and De Luca, A. (2014), “Secondary bracing systems for diagrid structures in tall buildings”, *Eng. Struct.*, **75**, 477-488. https://doi.org/10.1016/j.engstruct.2014.06.011.
- Moon, K.S. (2008), “Sustainable structural engineering strategies for tall buildings”, *Struct. Des. Tall Spec. Build.*, **17**(5), 895-914. https://doi.org/10.1002/tal.475.
- Moon, K.S., Connor, J.J. and Fernandez, J.E. (2007), “Diagrid structural systems for tall buildings: Characteristics and methodology for preliminary design”, *Struct. Des. Tall Spec. Build.*, **16**(2), 205-230. https://doi.org/10.1002/tal.311.
- Newmark, N.M. and Hall, W.J. (1982), “Earthquake spectra and design, EERI Monograph Series”, *Earthq. Eng. Res. Institute, Berkeley, C.A.*
- Nobahar, E., Farahi, M. and Mofid, M. (2016), “Quantification of seismic performance factors of the buildings consisting of disposable knee bracing frames”, *J. Construct. Steel Res.*, **124**, 132-141. https://doi.org/10.1016/j.jcsr.2016.05.007.
- Özkılıç, Y.O., Bozkurt, M.B. and Topkaya, C. (2018), “Evaluation of seismic response factors for BRBFs using FEMA P695 methodology”, *J. Construct. Steel Res.*, **151**, 41-57. https://doi.org/10.1016/j.jcsr.2018.09.015.
- Pejovic, J.R., Serdar, N.N. and Pejovic, R.R. (2017), “Optimal intensity measures for probabilistic seismic demand models of RC high-rise buildings”, *Earthq. Struct.*, **13**(3), 221-230. https://doi.org/10.12989/eas.2017.13.3.221.
- Pejovic, J.R., Serdar, N.N. and Pejovic, R.R. (2018), “Novel optimal intensity measures for probabilistic seismic analysis of RC high-rise buildings with core”, *Earthq. Struct.*, **15**(4), 443-452. https://doi.org/10.12989/eas.2018.15.4.443.
- Sadeghi, S. and Rofooei, F.R. (2018), “Quantification of the seismic performance factors for steel diagrid structures”, *J. Construct. Steel Res.*, **146**, 155-168. https://doi.org/10.1016/j.jcsr.2018.03.018.
- Shi, Q. and Zhang, F. (2019), “Simplified calculation of shear lag effect for high-rise diagrid tube structures”, *J. Build. Eng.*, **22**, 486-495. https://doi.org/10.1016/j.job.2019.01.009.
- Song, L.L. and Guo, T. (2017), “Probabilistic seismic performance assessment of self-centering prestressed concrete frames with web friction devices”, *Earthq. Struct.*, **12**(1), 109-118. https://doi.org/10.12989/eas.2017.12.1.109.
- Starossek, U. (2009), *Progressive collapse of structures*, London: thomas telford.
- Starossek, U.J.E.S. (2007), “Typology of progressive collapse”, *Eng. Struct.*, **29**(9), 2302-2307. https://doi.org/10.1016/j.engstruct.2006.11.025.
- Taranath, B. (2012), *Structural Analysis and Design of Tall Buildings, Steel and Composite Construction* CRC Press, Taylor & Francis, Group.
- Trabelsi, A., Kammoun, Z. and Beddey, A. (2017), “Seismic retrofitting of a tower with shear wall in UHPC based dune sand”, *Earthq. Struct.*, **12**(6), 591-601. https://doi.org/10.12989/eas.2017.12.6.591.
- Vamvatsikos, D. (2002), *Seismic performance, capacity and reliability of structures as seen through incremental dynamic analysis*, Citeseer.
- Vamvatsikos, D. and Cornell, C.A. (2002), “Incremental dynamic analysis”, *Earthq. Eng. Struct. Dyn.*, **31**(3), 491-514. https://doi.org/10.1002/eqe.141.
- Veismoradi, S. and Darvishan, E. (2018), “Probabilistic seismic assessment of mega buckling-restrained braced frames under near-fault ground motions”, *Earthq. Struct.*, **15**(5), 487-498. https://doi.org/10.12989/eas.2018.15.5.487.
- Vidic, T., Fajfar, P. and Fischinger, M. (1994), “Consistent inelastic design spectra: Strength and displacement”, *Earthq.*

- Eng. Struct. Dyn.*, **23**(5), 507-521.
<https://doi.org/10.1002/eqe.4290230504>.
- Whittaker, A., Hart, G. and Rojahn, C. (1999), "Seismic response modification factors", *J. Struct. Eng.*, **125**(4), 438-444.
[https://doi.org/10.1061/\(asce\)0733-9445\(1999\)125:4\(438\)](https://doi.org/10.1061/(asce)0733-9445(1999)125:4(438)).
- Zhang, C., Zhao, F. and Liu, Y. (2012), "Diagrid tube structures composed of straight diagonals with gradually varying angles", *Structural Des. Tall Spec. Build.*, **21**(4), 283-295.
<https://doi.org/10.1002/tal.596>.
- Zhao, F. and Zhang, C. (2015), "Diagonal arrangements of diagrid tube structures for preliminary design", *Struct. Des. Tall Spec. Build.*, **24**(3), 159-175. <https://doi.org/10.1002/tal.1159>.

KT